IOP PUBLISHING JOURNAL OF PHYSICS D: APPLIED PHYSICS

J. Phys. D: Appl. Phys. **41** (2008) 105204 (9pp) doi:10.1088/0022-3727/41/10/105204

Fluctuation charge effects in ionization fronts

Manuel Arrayás[1], J P Baltanás[2] and José L Trueba[1]

[1] Área de Electromagnetismo, Universidad Rey Juan Carlos, Camino del Molino s/n, 28943 Fuenlabrada, Madrid, Spain

[2] Departamento de Física Aplicada II, Universidad de Sevilla, Av. Reina Mercedes 2, 41012 Sevilla, Spain

Received 9 January 2008, in final form 7 March 2008
Published 8 April 2008
Online at stacks.iop.org/JPhysD/41/105204

Abstract

In this paper, we study the effects of charge fluctuations on the propagation of both negative and positive ionization fronts in streamer discharges. We show that fronts accelerate when random charge creation events are present. This effect might play a similar role to photoionization in order to make the front move faster.

(Some figures in this article are in colour only in the electronic version)

1. Introduction

A streamer is considered to be a plasma channel which propagates into a neutral gas. The discharge moves by ionizing the medium in front of its charged head due to a strong field induced by the head itself. These kinds of discharges produce sharp ionization waves that propagate into a non-ionized gas, leaving a non-equilibrium plasma behind [1]. The need of seed electrons ahead of the ionization fronts is critical for the propagation of positive streamers moving towards the anode. Raether [2] realized that Townsend's mechanism which takes into account the creation of extra charge by impact ionization [3] was not enough to explain the velocity of propagation of a streamer discharge. He pointed to photoionization as the process which enhances the propagation of the streamer. The role played by photoionization in the propagation of both negative and positive streamers has been studied in several works, experimentally and numerically [4–9].

In this work we show that charge fluctuations, whatever their physical nature related to thermal noise, terrestrial or cosmic radiation, impurities in the gas, residual charge, etc [10], can play the same role as photoionization concerning front propagation. More precisely, fluctuations will make the front move faster when they are spread out over the whole region occupied by the gas.

A natural way of modelling the charge fluctuations is to consider random initial conditions. Consequently, we will take an initial charge distribution function and add a perturbation generated at random. For each realization of the random term, the temporal evolution of the streamer will be given by an effective simplified model widely used in deterministic numerical simulations. Finally, we will calculate averaged quantities as the mean values over the total number of realizations. Thus, we compare the contribution of the fluctuations to the propagation velocity of the fronts for different cases, expecting that the average behaviour of the front over random initial conditions will describe appropriately the real situation in which free charges are created or destroyed at every point of the gas at any time during the discharge process. It will be shown that fluctuations in the charge distribution lead to important effects. In order to discard the possibility of this contribution being a consequence of adding extra charge, we do a second kind of numerical experiment where we compare the results of a deterministic case with the stochastic one keeping the same total charge on average. In both cases, we will see that the effects of fluctuations on streamer dynamics can be understood from a theoretical point of view.

The outline of the paper is as follows. In section 2 we review the derivation of a simplified model which includes photoionization, diffusion and impact ionization terms. We take a standard model for streamers and the parameter values normally used for atmospheric discharges and simplify it taking special care to keep the relevant physics. In section 3 the particular case of the planar geometry is considered. For this case, the photoionization term can be approximated and the numerical simulations are simplified. We introduce in section 4 the random initial conditions in order to model the fluctuations in the charge density as the front develops. We solve the minimal set of equations numerically for different realizations of the initial charge distribution and then we take the average over the number of realizations. This procedure allows us to

study the role played by charge fluctuations in the streamer dynamics.

In section 5 two cases are considered. In the first one, the photoionization term is included, whereas in the second one its effects are neglected. Thus we can test the contribution of the charge fluctuations to the front propagation. The front accelerates due to the presence of the fluctuations, even without photoionization. More numerical experiments in section 6 reveal the role of charge fluctuations more clearly. When the fluctuations are introduced, we discard negative values of the charge density, so the physical requirement of the positiveness of the charge densities is fulfilled. Thus, the question of whether the acceleration of the front is a consequence of the randomness of the initial conditions or whether it is related to the addition of extra charge on average naturally arises. We present other numerical experiments to elucidate this important fact. The results yield the same increasing effect for the velocity of propagation. In section 7 the results are analysed and the conditions under which the fluctuations play the same role as photoionization are discussed. Finally, we present some concluding remarks.

2. Streamer discharge model

In this section, we recall a simplified fluid description of a weakly ionized plasma based on kinetic theory. We start from a model which has been extensively used in numerical simulations and seems to capture the essential physics of a streamer discharge [11, 12]. The model including photoionization, S^{ph}, reads [13, 14]

$$\frac{\partial N_{\mathrm{e}}}{\partial \tau} = \nabla_{\boldsymbol{R}} \cdot (\mu_{\mathrm{e}} \boldsymbol{\mathcal{E}} N_{\mathrm{e}} + D_{\mathrm{e}} \nabla_{\boldsymbol{R}} N_{\mathrm{e}}) + (\nu_{\mathrm{i}} - \nu_{\mathrm{a}} - \nu_{\mathrm{ep}} N_{\mathrm{p}}) N_{\mathrm{e}} + S^{\mathrm{ph}}, \tag{1}$$

$$\frac{\partial N_{\mathrm{p}}}{\partial \tau} = (\nu_{\mathrm{i}} - \nu_{\mathrm{ep}} N_{\mathrm{p}}) N_{\mathrm{e}} - \nu_{\mathrm{np}} N_{\mathrm{n}} N_{\mathrm{p}} + S^{\mathrm{ph}}, \tag{2}$$

$$\frac{\partial N_{\mathrm{n}}}{\partial \tau} = \nu_{\mathrm{a}} N_{\mathrm{e}} - \nu_{\mathrm{np}} N_{\mathrm{n}} N_{\mathrm{p}}, \tag{3}$$

in which τ is time, $\boldsymbol{R}$ is the position in space and $\nabla_{\boldsymbol{R}}$ refers to spatial derivatives, N_{e} is the electron density, N_{p} the positive ion density, N_{n} the negative ion density, μ_{e} and D_{e} are the mobility and diffusion coefficient of the electrons, ν_{i} is the ion production rate, ν_{ep} and ν_{np} are the recombination coefficients and ν_{a} the attachment rate coefficient. The electric field $\mathcal{E}$ is given by Poisson's equation,

$$\nabla_{\boldsymbol{R}} \cdot \boldsymbol{\mathcal{E}} = \frac{e}{\varepsilon_0}(N_{\mathrm{p}} - N_{\mathrm{n}} - N_{\mathrm{e}}), \tag{4}$$

where e is the absolute value of the electron charge and ε_0 is the permittivity of the gas.

For the ionization coefficient ν_{i}, we take the phenomenological approximation given by Townsend [3]

$$\nu_{\mathrm{i}} = \mu_{\mathrm{e}} |\boldsymbol{\mathcal{E}}| \alpha_0 \exp\left(\frac{-\mathcal{E}_0}{|\boldsymbol{\mathcal{E}}|}\right), \tag{5}$$

where μ_{e} is the electron mobility, α_0 is the inverse of ionization length and $\mathcal{E}_0$ is the characteristic impact ionization electric field.

The photoionization term S^{ph} in equations (1) and (2) involves a non-local contribution. For nitrogen–oxygen mixtures it is written [4, 15] as

$$S_{\mathrm{ph}}(\boldsymbol{R}) = S_0 \int \nu_{\mathrm{i}}(\boldsymbol{R}') N_{\mathrm{e}}(\boldsymbol{R}') K_{\mathrm{ph}}(|\boldsymbol{R} - \boldsymbol{R}'|)\, \mathrm{d}^3 R', \tag{6}$$

where S_0 is given by

$$S_0 = \frac{1}{4\pi} \frac{p_{\mathrm{q}}}{p + p_{\mathrm{q}}} \xi \left(\frac{\nu_*}{\nu_{\mathrm{i}}}\right) \frac{1}{\ln(\chi_{\max}/\chi_{\min})}. \tag{7}$$

In this expression, p_{q} is the quenching pressure of the singlet states of N_2, p is the gas pressure, ξ is the average photoionization efficiency in the interval of radiation frequencies relevant to the problem, ν_* is the effective excitation coefficient for N_2 state transitions from which the ionization radiation comes out and $\chi_{\min}$ and $\chi_{\max}$ are, respectively, the minimum and the maximum absorption cross sections of O_2 in the relevant radiation frequency interval. In addition, ν_* can be considered to be proportional to ν_{i} for the high values of the ionization electric field considered in this work [4].

The kernel $K_{\mathrm{ph}}(|\boldsymbol{R} - \boldsymbol{R}'|)$ reads [5]

$$K_{\mathrm{ph}}(R) = \frac{\exp(-\chi_1 R) - \exp(-\chi_2 R)}{R^3}, \tag{8}$$

in which $\chi_1 = \chi_{\min} p_{\mathrm{O_2}}$ and $\chi_2 = \chi_{\max} p_{\mathrm{O_2}}$, $p_{\mathrm{O_2}}$ being the partial pressure of oxygen in air, so that $\chi_1 < \chi_2$.

In atmospheric discharges, we have the following orders of magnitude for the different coefficients of the model [4]: the term ν_{i} is of the order of $10^{10}\ \mathrm{s}^{-1}$ for large electric fields, ν_{a} is about $10^{8}\ \mathrm{s}^{-1}$ and ν_{ep} and ν_{np} are about $10^{-13}\ \mathrm{m}^3\ \mathrm{s}^{-1}$. Moreover, N_{p} is of the same order of N_{e}. For these parameter values we now will turn to see that to solve numerically the system (1)–(4) is equivalent to solving a reduced one. To this end, we will proceed in successive steps.

First, as we have seen, $\nu_{\mathrm{a}} \ll \nu_{\mathrm{i}}$, so that the term $\nu_{\mathrm{a}} N_{\mathrm{e}}$ can be discarded from equation (1) in a first approximation. Second, in the stationary regime, equation (3) leads to $N_{\mathrm{n}} \sim \nu_{\mathrm{a}}/\nu_{\mathrm{np}} \sim 10^{21}\ \mathrm{m}^{-3}$. So we can neglect the term $\nu_{\mathrm{np}} N_{\mathrm{n}} N_{\mathrm{p}}$ in equation (2) by comparison with the term $\nu_{\mathrm{i}} N_{\mathrm{e}}$. As a consequence, within this approximation, equation (3) decouples from (1) to (2), implying that N_{n} remains almost constant while N_{e} and N_{p} grow up to their saturation values. Thus, the contribution of N_{n} to the Poisson equation (4) can be interpreted as part of the initial condition for the electric field. Taking all this into account, the model reads

$$\frac{\partial N_{\mathrm{e}}}{\partial \tau} = \nabla_{\boldsymbol{R}} \cdot (\mu_{\mathrm{e}} \boldsymbol{\mathcal{E}} N_{\mathrm{e}} + D_{\mathrm{e}} \nabla_{\boldsymbol{R}} N_{\mathrm{e}}) + (\nu_{\mathrm{i}} - \nu_{\mathrm{ep}} N_{\mathrm{p}}) N_{\mathrm{e}} + S^{\mathrm{ph}}, \tag{9}$$

$$\frac{\partial N_{\mathrm{p}}}{\partial \tau} = (\nu_{\mathrm{i}} - \nu_{\mathrm{ep}} N_{\mathrm{p}}) N_{\mathrm{e}} + S^{\mathrm{ph}}, \tag{10}$$

$$\nabla_{\boldsymbol{R}} \cdot \boldsymbol{\mathcal{E}} = \frac{e}{\varepsilon_0}(N_{\mathrm{p}} - N_{\mathrm{e}}). \tag{11}$$

Finally, we compare $\nu_{\mathrm{ep}} N_{\mathrm{e}} N_{\mathrm{p}}$ with the term $\nu_{\mathrm{i}} N_{\mathrm{e}}$ both in equations (9) and (10). Initially, the value of N_{p} is close to

zero, so that we can use the Poisson equation (11) to write equation (9) as

$$\frac{\partial N_e}{\partial \tau} - \mu_e \boldsymbol{\mathcal{E}} \cdot \nabla_{\boldsymbol{R}} N_e - D_e \nabla^2_{\boldsymbol{R}} N_e = \left[\nu_i + \mu_e \frac{e}{\varepsilon_0}(N_p - N_e) \right] N_e + S^{ph}. \quad (12)$$

From this expression, we can see that, since S^{ph} has a small effect, the total populations of both ions and electrons can grow only up to a saturation value at which $\nu_i + \mu_e e/\varepsilon_0 (N_p - N_e) = 0$, so that, at all times, the following inequality holds:

$$N_e - N_p \leqslant \frac{\nu_i \varepsilon_0}{\mu_e e} \sim 10^{20}\ \mathrm{m}^{-3}. \quad (13)$$

Therefore, since $\nu_{ep} N_e N_p \ll \nu_i N_e$, our final simplified model reads:

$$\frac{\partial N_e}{\partial \tau} = \nabla_{\boldsymbol{R}} \cdot (\mu_e \boldsymbol{\mathcal{E}} N_e + D_e \nabla_{\boldsymbol{R}} N_e) + \nu_i N_e + S^{ph}, \quad (14)$$

$$\frac{\partial N_p}{\partial \tau} = \nu_i N_e + S^{ph}, \quad (15)$$

$$\nabla_{\boldsymbol{R}} \cdot \boldsymbol{\mathcal{E}} = \frac{e}{\varepsilon_0}(N_p - N_e). \quad (16)$$

Let us remark that the orders of magnitude deduced for N_e and N_p coincide with those found in full numerical simulations by Liu and Pasko [4].

3. Planar fronts

We now turn our attention to the particular case of a planar front. For this case, we will show how the photoionization term can be written in an approximated form especially useful in numerical experiments.

Let us begin by writing the model given by equations (14)–(16) in dimensionless units. Natural units are given by the ionization length $R_0 = \alpha_0^{-1}$, the characteristic impact ionization field $\mathcal{E}_0$ and the electron mobility μ_e, which lead to the velocity scale $U_0 = \mu_e \mathcal{E}_0$, and the time scale $\tau_0 = R_0/U_0$. We introduce the dimensionless variables $\boldsymbol{r} = \boldsymbol{R}/R_0$, $t = \tau/\tau_0$, the dimensionless field $\boldsymbol{E} = \boldsymbol{\mathcal{E}}/\mathcal{E}_0$, the dimensionless electron and positive ion particle densities $n_e = N_e/N_0$ and $n_p = N_p/N_0$, with $N_0 = \varepsilon_0 \mathcal{E}_0/(eR_0)$ and the dimensionless diffusion constant $D = D_e/(R_0 U_0)$. Then, the dimensionless evolution equations for n_e and n_p read

$$\frac{\partial n_e}{\partial t} = \nabla \cdot (n_e \boldsymbol{E} + D \nabla n_e) + n_e |\boldsymbol{E}| \mathrm{e}^{-1/|\boldsymbol{E}|} + S, \quad (17)$$

$$\frac{\partial n_p}{\partial t} = n_e |\boldsymbol{E}| \mathrm{e}^{-1/|\boldsymbol{E}|} + S, \quad (18)$$

where S is the dimensionless photoionization source term

$$S(\boldsymbol{r}) = S_0 \int n_e(\boldsymbol{r}') |\boldsymbol{E}(\boldsymbol{r}')| \mathrm{e}^{-1/|\boldsymbol{E}(\boldsymbol{r}')|} K(|\boldsymbol{r} - \boldsymbol{r}'|)\, \mathrm{d}^3 r', \quad (19)$$

and

$$S_0 = \frac{1}{4\pi} \frac{p_q}{p + p_q} \xi \left(\frac{\nu_*}{\nu_i} \right) \frac{1}{\ln(\chi_{max}/\chi_{min})}. \quad (20)$$

Also,

$$K(r) = \frac{\exp(-(\chi_1/\alpha_0)r) - \exp(-(\chi_2/\alpha_0)r)}{r^3}. \quad (21)$$

Now we restrict ourselves to a planar geometry, in which the evolution of the ionization front is along the z-axis. In this case, the photoionization source term can be written as

$$S(z) = S_0 \int \mathrm{d}z' n_e(z', t) |\boldsymbol{E}(z', t)| \mathrm{e}^{-1/|\boldsymbol{E}(z', t)|} I(|z - z'|), \quad (22)$$

where

$$I(|z - z'|) = \int_{-\infty}^{\infty} \mathrm{d}y' \int_{-\infty}^{\infty} \mathrm{d}x' \frac{1}{(x'^2 + y'^2 + (z - z')^2)^{3/2}} \times \left(\mathrm{e}^{(-(\chi_1/\alpha_0)\sqrt{x'^2 + y'^2 + (z - z')^2})} - \mathrm{e}^{(-(\chi_2/\alpha_0)\sqrt{x'^2 + y'^2 + (z - z')^2})} \right). \quad (23)$$

Changing to cylindrical coordinates, and integrating in the polar angle, equation (23) results in

$$I(s) = 2\pi \int_s^{\infty} \mathrm{d}w \frac{\exp(-(\chi_1/\alpha_0)w) - \exp(-(\chi_2/\alpha_0)w)}{w^2}, \quad (24)$$

where $s = |z - z'|$ and $w = \sqrt{r^2 + s^2}$. Defining the quantities

$$\varphi_0 = 2\pi S_0 = \frac{1}{2} \frac{p_q}{p + p_q} \xi \left(\frac{\nu_*}{\nu_i} \right) \frac{1}{\ln(\chi_{max}/\chi_{min})}, \quad (25)$$

and

$$k(s) = \frac{I(s)}{2\pi}, \quad (26)$$

we can write the dimensionless photoionization term in the planar case as

$$S(z) = \varphi_0 \int \mathrm{d}z' n_e(z', t) |\boldsymbol{E}(z', t)| \mathrm{e}^{-1/|\boldsymbol{E}(z', t)|} k(z - z'), \quad (27)$$

where

$$k(s) = \int_{s/\alpha_0}^{\infty} \mathrm{d}x \frac{\exp(-\chi_1 x) - \exp(-\chi_2 x)}{\alpha_0 x^2}. \quad (28)$$

The function $k(s)$ cannot be computed explicitly in terms of elementary functions, but its asymptotic behaviour can be calculated. For $s \to \infty$, we have

$$k(s) \simeq \frac{\mathrm{e}^{-(\chi_1/\alpha_0)s}}{(\chi_1/\alpha_0)s^2} - \frac{\mathrm{e}^{-(\chi_2/\alpha_0)s}}{(\chi_2/\alpha_0)s^2}, \quad (29)$$

and for $s \to 0$, it is

$$k(s) \simeq \frac{\chi_1 - \chi_2}{\alpha_0} \ln s + \text{const.} \quad (30)$$

In the numerical computations, we will approximate the function $k(s)$ by functions with the same behaviour at infinity and zero as the ones shown in equations (29) and (30). The simulations show that the results are insensitive to the details of these approximations and depend only on the behaviour at zero and infinity. In fact, we will use a kernel such that it is equal to equation (30) for $s < 1$ and it is equal to equation (29)

for $s > 1$. The constant in equation (30) will be chosen in such a way that $k(s)$ is continuous at $s = 1$.

Following [4, 6], we will take for the simulations $\xi(\nu_*/\nu_i) = 0.1$, $p_q = 30\,\mathrm{Torr}$, $\chi_1 = 0.035\,\mathrm{Torr}^{-1}\,\mathrm{cm}^{-1}\,p_{O_2}$, and $\chi_2 = 2\,\mathrm{Torr}^{-1}\,\mathrm{cm}^{-1}\,p_{O_2}$. We will assume the partial pressure of the oxygen in air is given by $p_{O_2} = \gamma p$, where p is the total pressure and γ a pure number between zero and one. For the inverse ionization length α_0 we will take the value for nitrogen that depends on pressure as $\alpha_0 = 5.8\,\mathrm{Torr}^{-1}\,\mathrm{cm}^{-1}\,p$ [16]. For the diffusion coefficient we take $D_e = 0.1\,\mathrm{m}^2\,\mathrm{s}^{-1}$ [12].

Using these values it turns out

$$\varphi_0 = 0.37\frac{1}{30+p}, \tag{31}$$

with p expressed in Torr, and

$$k(s) = \begin{cases} \dfrac{\exp(-0.006\,\gamma s)}{(0.006\,\gamma)s^2} - \dfrac{\exp(-0.34\,\gamma s)}{(0.34\,\gamma)s^2}, \\ \qquad s > 1, \\ -0.34\,\gamma \ln s + \dfrac{\exp(-0.006\,\gamma)}{(0.006\,\gamma)} - \dfrac{\exp(-0.34\,\gamma)}{(0.34\,\gamma)}, \\ \qquad s \leqslant 1. \end{cases} \tag{32}$$

Finally, we take the electric field as $\boldsymbol{E} = -E\boldsymbol{u}_z$, E being its modulus. Thus the system of equations that we will study in the planar case turns out to be

$$\frac{\partial n_e}{\partial t} = -\frac{\partial}{\partial z}\left(n_e E - D\frac{\partial n_e}{\partial z}\right) + n_e E\,\mathrm{e}^{-1/E} + S, \tag{33}$$

$$\frac{\partial n_p}{\partial t} = n_e E\,\mathrm{e}^{-1/E} + S, \tag{34}$$

$$n_p - n_e = -\frac{\partial E}{\partial z}, \tag{35}$$

where S is the photoionization term given by (27).

The system of equations (33)–(35) can be written in a more convenient way for our numerical simulations. To this end, we subtract equation (33) from equation (34), thus obtaining

$$\frac{\partial n_p}{\partial t} - \frac{\partial n_e}{\partial t} = \frac{\partial}{\partial z}\left(n_e E - D\frac{\partial n_e}{\partial z}\right). \tag{36}$$

In addition, by taking partial derivatives in equation (35) we have

$$\frac{\partial n_p}{\partial t} - \frac{\partial n_e}{\partial t} = -\frac{\partial}{\partial t}\left(\frac{\partial E}{\partial z}\right) = \frac{\partial}{\partial z}\left(-\frac{\partial E}{\partial t}\right). \tag{37}$$

After comparing both equations, we arrive at an evolution equation for the electric field

$$\frac{\partial E}{\partial t} = D\frac{\partial n_e}{\partial z} - n_e E. \tag{38}$$

This equation, together with equation (33), constitutes an appropriate starting point to analyse the minimal model numerically. In summary, we consider the equations

$$\frac{\partial n_e}{\partial t} = -\frac{\partial}{\partial z}\left(n_e E - D\frac{\partial n_e}{\partial z}\right) + n_e E\,\mathrm{e}^{-1/E} + S, \tag{39}$$

$$\frac{\partial E}{\partial t} = D\frac{\partial n_e}{\partial z} - n_e E, \tag{40}$$

which will be solved by means of a finite difference method with a given initial distribution $n_{e,0}(z) = n_e(z, 0)$ and electric field E_0.

4. Random initial conditions

In this section, we will introduce random initial conditions in order to model the fluctuations in the charge density as the fronts develop. By this, we mean that $n_{e,0}(z)$ will be written as the sum of a smooth deterministic term and a perturbation generated at random

$$n_{e,0}(z) = n_{e,0}^{(\mathrm{det})}(z) + n_{e,0}^{(\mathrm{random})}(z), \tag{41}$$

where $n_{e,0}^{(\mathrm{det})}(z)$ is the deterministic term of the form considered in [13]

$$n_{e,0}^{(\mathrm{det})}(z) = n_0 z\,\mathrm{e}^{-(z-z_0)^2/\sigma}, \tag{42}$$

which mimics the initial seed of charge developing into a streamer[3], and $n_{e,0}^{(\mathrm{random})}(z)$ is the dimensionless random term

$$n_{e,0}^{(\mathrm{random})}(z) = \sqrt{\Delta}\eta(z), \tag{43}$$

which introduces the charge fluctuations, whatever its origin (thermal noise, radiation, etc). In this equation, $\eta(z)$ will be obtained, for each z, from a zero mean Gaussian distribution with unit variance, Δ representing the intensity of the fluctuations in the initial electron density. From the above definition, it is clear that $n_{e,0}(z)$ might take both positive and negative values. Of course, a negative electron density lacks any physical meaning. So, when generating the initial distribution $n_{e,0}(z)$, we check the condition $n_{e,0}(z) > 0$ for every z. In case we obtain $n_{e,0}(z) \leqslant 0$ for some $z = z'$, we redefine $n_{e,0}(z') = 0$.

It is clear that we can obtain different initial conditions $n_{e,0}(z)$, all of them with the same deterministic term and the same Δ, just choosing different values of $\eta(z)$ for each z from the Gaussian distribution mentioned above. We will call each of the initial conditions generated by following this procedure a realization. Of course, the solution of the streamer discharge model will change for different realizations. Thus, in order to analyse the role played by charge fluctuations in the evolution of the front, we look at the averaged response of the system to the random initial condition. More precisely, the set of equations of the model will be solved starting from different realizations of the initial conditions and, after this, the quantities of interest (in our case, the positions of the fronts as a function of time) will be evaluated for each of the initial solutions and the average over realizations computed numerically. As we pointed out in the introduction, it is expected that the response of the system to the presence of charge fluctuations in a real case will be conveniently mimicked by this average procedure.

[3] We have checked that replacing the right-hand term in equation (42) by a Gaussian distribution produces similar results to those presented in this work.

5. Acceleration of fronts due to random initial conditions

In this section we will show the results of our numerical experiments. We consider the case in which a divergence-free electric field $\boldsymbol{E}_0 = -E_0\boldsymbol{u}_z$ is set along the z-axis, so that electrons move towards the positive z-axis direction. We will see how the randomly distributed charge affects the front propagation in a similar way as the photoionization term does. We will consider here two separate cases. In the first one, the photoionization term will be included, whereas in the second one its effects will be neglected. Thus we can test the contribution of the charge fluctuations to the front propagation.

5.1. *Effects of the fluctuations on the front propagation*

We are going to test the effects of the charge fluctuations on the streamer propagation including photoionization. In our first numerical experiment we take $D = 0.57$, $p = 750$ Torr, $\gamma = 0.25$ and solve the equations given by (39) and (40). The initial value of the electric field is $E_0 = 2$ in the simulations. Following [16], the unit of the electric field is 2×10^7 V m^{-1}, the length unit 2.3×10^{-6} m and the time unit 3×10^{-12} s. For particle densities, the unit is 4.7×10^{20} m^{-3}.

A finite difference method with a spatial step size Δz and a time step Δt is used to follow the time evolution of $n_e(z,t)$ and $E(z,t)$. More precisely, for each time step, the spatial derivatives appearing at the right hand sides of equations (39) and (40) are approximated as the differences

$$\frac{\partial n_e(z,t)}{\partial z} = \frac{n_e(z+\Delta z,t) - n_e(z-\Delta z,t)}{2\Delta z}, \tag{44}$$

$$\frac{\partial^2 n_e(z,t)}{\partial z^2} = \frac{n_e(z+\Delta z,t) + n_e(z-\Delta z,t) - 2n_e(z,t)}{(\Delta z)^2}, \tag{45}$$

and

$$\frac{\partial}{\partial z}[n_e(z,t)E(z,t)] = \frac{n_e(z+\Delta z,t)E(z+\Delta z,t) - n_e(z-\Delta z,t)E(z-\Delta z,t)}{2\Delta z}, \tag{46}$$

while the integral appearing in equation (27), which defines the dimensionless photoionization term $S(z)$, is replaced by a discrete sum over Δz. The use of these expressions makes the evaluation of $\partial n_e(z,t)/\partial t$ and $\partial E(z,t)/\partial t$ straightforward within this approximation. Finally, the solution at time $t + \Delta t$ is given by

$$n_e(z, t+\Delta t) = n_e(z,t) + \left[\frac{\partial n_e(z,t)}{\partial t}\right]\Delta t, \tag{47}$$

$$E(z, t+\Delta t) = E(z,t) + \left[\frac{\partial E(z,t)}{\partial t}\right]\Delta t. \tag{48}$$

The respective values of the spatial and temporal intervals are chosen to be $\Delta z = 0.01$ and $\Delta t = 0.000\,04$, thus ensuring that the stability criterion $2D\Delta t/(\Delta z)^2 < 1$ is fulfilled. In addition, the initial values of the electric field and electron density used in the simulations are given, respectively, by $E_0 = 2$ and equations (41)–(43) with $n_0 = 1/3$, $z_0 = 10$, $\sigma = 0.1$ and $\Delta = 0.001$.

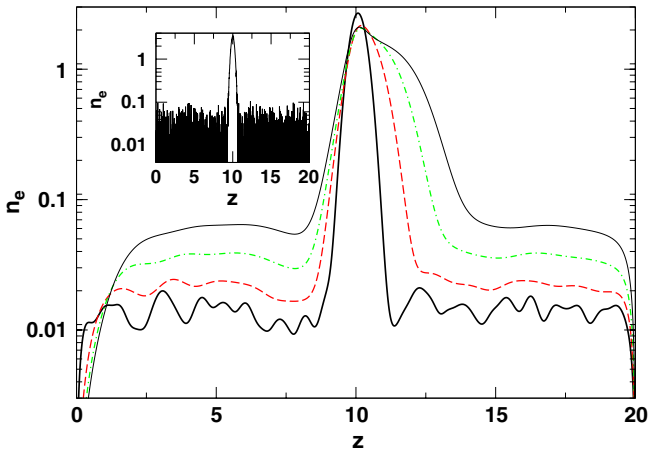

Figure 1. Log scale plot of the evolution of the electron charge density n_e for one realization of the stochastic initial conditions when diffusion and photoionization are both present. Values of the parameters of the initial condition (depicted in the inset in logarithmic scale also) are $n_0 = 1/3$, $z_0 = 10$, $\sigma = 0.1$ and $\Delta = 0.001$. The propagation of two fronts can be seen at $t = 0.04$ (thick line), $t = 0.2$ (dashed line), $t = 0.4$ (dotted–dashed line) and $t = 0.6$ (thin line).

In figure 1, we plot the electron density at different times for the particular realization of the initial conditions shown in the inset. Logarithmic scale is used in this figure in order to make more visible the development of two fronts during the initial state of the streamer propagation. The evolution of two fronts is clearly seen, one of them moving towards the anode located on the right, which we call the negative front, and the other one towards the opposite direction, named the positive front [13].

We can track the motion of the negative and positive fronts by looking at the time evolution of the point $z^\star(t)$ at which the electron density has a given value. We have chosen a level of $n_e = 0.1$.[4] Due to the random character of the initial condition, different electron densities profiles develop, corresponding to different realizations of the random part in equation (41), even for fixed values of Δ. When, for each of these realizations, $z^\star$ is plotted as a function of time, a virtually linear dependence is obtained once a relatively short transient period elapses, thus resembling the results given in [13]. Of course, the exact linear dependence varies slightly from one realization to another. However, it is straightforward to obtain the average linear dependence from the set of realizations run in simulations. This average provides an idea on the effect of the fluctuations on the development of the fronts. In figure 2, we compare the graphs of $z^\star(t)$, averaged over 25 realizations, corresponding to different values of the fluctuation term in the initial charge distribution. The effect of charge fluctuations is an acceleration of the front propagation which reaches a higher, though still constant, velocity. It is apparent that the front accelerates when the intensity Δ increases.

[4] The simulations show that the results are insensitive to the choice of this value within certain reasonable limits.

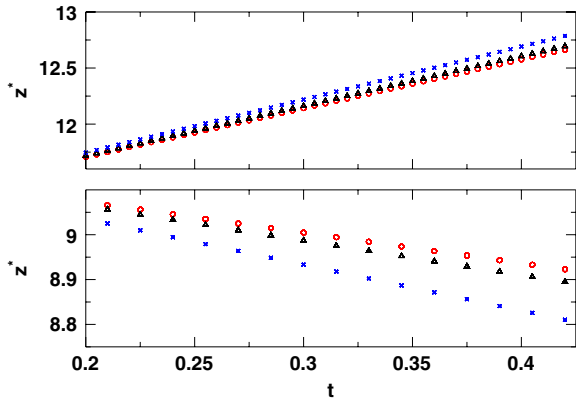

Figure 2. Evolution of the averaged $z^\star(t)$ for different values of Δ when diffusion and photoionization are both present, corresponding to negative (upper panel) and positive (lower panel) fronts. Empty circles stand for $\Delta = 10^{-6}$, triangles for $\Delta = 10^{-4}$ and crosses for $\Delta = 10^{-3}$.

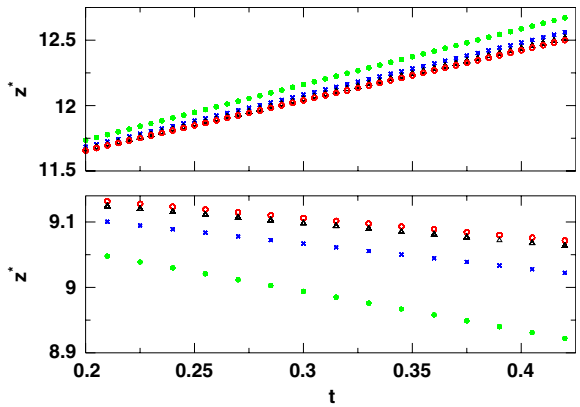

Figure 3. Evolution of $z^\star(t)$ for different values of Δ when photoionization is absent. The positions of negative (upper panel) and positive (lower panel) fronts have been tracked for different values of Δ: 10^{-5} (empty circles), 10^{-4} (triangles), 10^{-3} (crosses) and 5×10^{-3} (full points).

5.2. Acceleration without photoionization

Now we will switch off the effect of the photoionization in order to see the singular contribution of the fluctuations to the front motion.

Figure 3 shows that the effect of increasing the speed of the propagation persists in the absence of the photoionization term. In this figure we depict the averaged $z^\star(t)$ over $N = 50$ realizations as a function of time for different values of Δ and for the same set of parameter values as in the previous section, but in the absence of the photoionization term ($\varphi = 0$). Clearly, the front accelerates as a consequence of the presence of the fluctuations when Δ increases, even without photoionization.

6. Numerical experiments with the same initial charge

A further numerical experiment will reveal the role of charge fluctuations more clearly. It is apparent that the procedure used above to introduce the random term in the initial condition is biased. This is caused by the physical requirement of the positiveness of the electron density. When the fluctuations are introduced the total initial electronic charge is increased. Thus, the question if the acceleration of the front is a consequence of the randomness of the initial conditions or it is related to the addition of charge on average naturally arises. We present here another numerical experiment to elucidate this important fact.

The total number of electrons introduced at time $t = 0$ in the region between the plates is given by

$$\mathcal{N}_e = \int dz n_{e,0}(z), \tag{49}$$

where the integral is performed over the whole z-domain. Given a fully deterministic initial electron density of the form given in equation (42), i.e.

$$n_{e,0}(z) = n_{e,0}^{(det)}(z) = n_0 z\, e^{-(z-z_0)^2/\sigma}, \tag{50}$$

it is clear that, for a fixed z_0, the total number of electrons $\mathcal{N}_e$ can be easily changed by modifying n_0, σ or both (an analytical expression in terms of error functions can be obtained for the above integral evaluated in a closed interval). On the other hand, the averaged initial number of electrons introduced in the system when the random term is present (see equation (41)) is also easily calculated numerically as the total number of electrons introduced in all the realizations over the number of realizations.

The following numerical experiment will allow us to compare the deterministic case with the stochastic one, while the total initial electron charge is the same in both cases. For every value of Δ, we compute numerically the average initial number of electrons introduced in the system by means of the initial condition (41). Let us call this number $\bar{\mathcal{N}}_e$. Then we modify n_0 or σ in equation (42) in order to obtain a purely deterministic initial condition with the same number of initial electrons, i.e. we look for a value of n_0 or σ satisfying

$$\int dz n_{e,0}^{(det)}(z) = \bar{\mathcal{N}}_e. \tag{51}$$

After this, we follow the time evolution of the front starting from both initial conditions, the deterministic and the stochastic one, which have the same total initial charge (in average). The results are included in figures 4–7. For convenience, we have treated separately the cases in which n_0 is changed from those in which σ is modified.

6.1. Changing the width of the initial distribution

We consider first the case in which σ in equation (50) is varied, keeping the prefactor n_0 constant. Initially, we take into account both photoionization and diffusion. The position of $z^\star$ as a function of time for a level $n_e = 0.1$ is plotted in figure 4, where upper (lower) panels stand for negative (positive) fronts. In this figure, we use stars to plot the averaged position of the front over 25 different realizations of the initial condition, evaluated as explained in the previous section, for Δ values 10^{-4} (left panels) and 5×10^{-3} (right panels). With

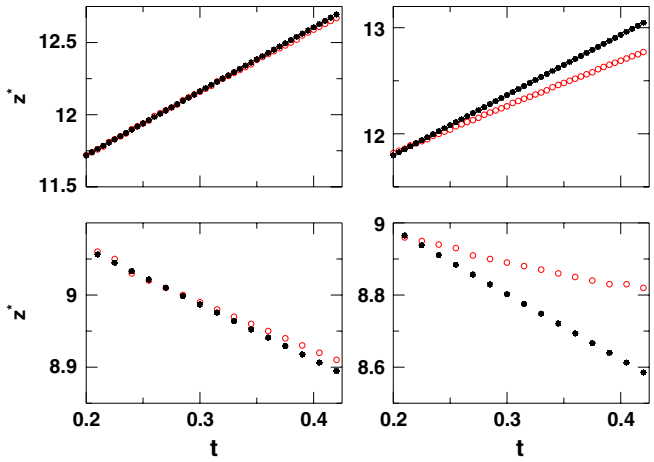

Figure 4. Position of negative and positive fronts as a function of time in the presence of photoionization and a random initial condition. Full points correspond to the averaged response of the system under random initial conditions. The evolution from a deterministic initial condition of the form in equation (42), where σ is chosen to fulfil equation (51), has been plotted with empty circles. $\Delta = 10^{-4}$ for the left panels and $\Delta = 5 \times 10^{-3}$ for the right ones.

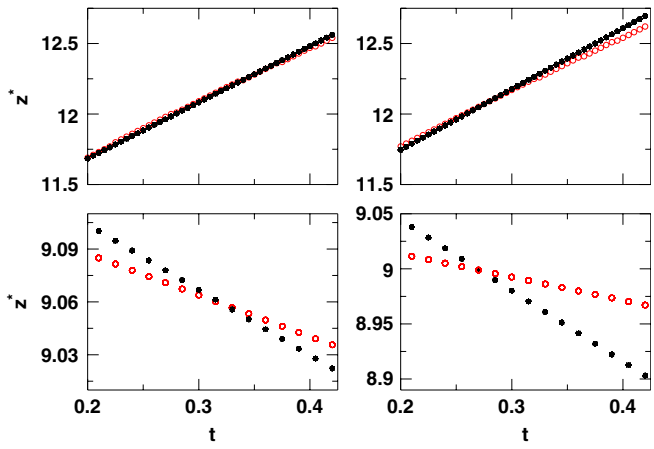

Figure 5. Position of negative and positive fronts as a function of time in the absence of the photoionization term. Full points correspond to the averaged response of the system under random initial conditions. The evolution from a deterministic initial condition of the form in equation (42), where σ is chosen to fulfil equation (51), has been plotted with empty circles. $\Delta = 10^{-3}$ for the left panels and $\Delta = 6 \times 10^{-3}$ for the right ones.

empty circles, we plot the values of $z^\star(t)$ corresponding to purely deterministic initial conditions of the form given in equation (42), with $z_0 = 10$ and $n_0 = 1/3$. Moreover, for each Δ, σ is computed by imposing that equation (51) holds, where $\bar{\mathcal{N}}_e$ is defined as the average over realizations of the total initial charge corresponding to the random initial condition with $\Delta = 10^{-4}$ and $\Delta = 5 \times 10^{-3}$, respectively.

As in the previous section, it is apparent that the speed of both positive and negative fronts is higher in the random case than in the deterministic one. At the same time, the accelerating effect is higher as Δ increases. However, this numerical experiment confirms that the acceleration of the fronts is truly a consequence of the random distribution of the initial charge and not a spurious effect caused by the addition of new charge to the initial situation.

In figure 5, after averaging over 50 realizations, we show that the effect persists in the absence of the photoionization term. It can be seen that the velocity of propagation given by the slope of the numerical data increases. It can be observed a cross of the dot and circle lines. This fact simply reflects that the initial point for the level $z^\star$ in the deterministic initial condition case and the initial point for the level $z^\star$ in the random initial condition case are different.

6.2. *Changing the prefactor*

Now we will change the prefactor n_0 defined in equation (50), keeping σ constant. In figure 6, the positions $z^\star(t)$ corresponding to random and deterministic initial conditions with the same initial charge (in average) are drawn. We consider the cases in which the prefactor n_0 in equation (42) is tuned to satisfy equation (51) when $\Delta = 10^{-4}$ (left panels) and $\Delta = 5 \times 10^{-3}$ (right panels), while the rest of the parameters are kept fixed.

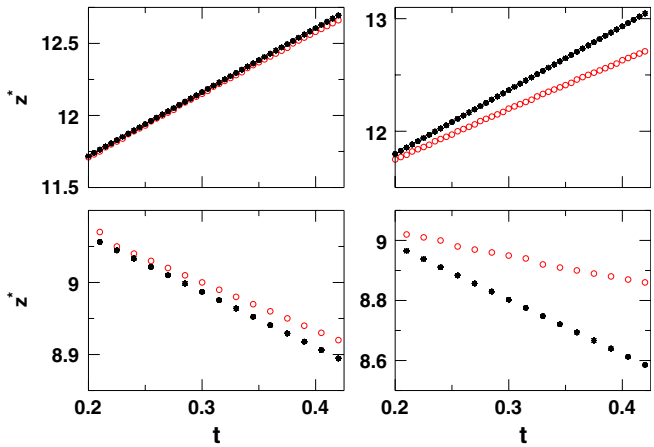

Figure 6. The same as in figure (4), with fixed σ and corresponding values of n_0 fulfilling equation (51) when $\Delta = 10^{-4}$ (left panels) and $\Delta = 5 \times 10^{-3}$ (right panels).

The results for the negative and the positive fronts are very similar to those described in the previous section, confirming that, starting from the same total initial charge, the fronts propagate faster in those cases in which the fluctuations due to uncontrollable environmental sources are present. The speed of the fronts depends on the strength of the fluctuations.

Again, the results are confirmed when the photoionization term is switched off, as can be seen in figure 7. This fact clearly shows that the presence of sparse charge throughout the gap between the electrodes due to natural sources provides an accelerating mechanism by itself, in addition to that of photoionization.

7. Analysis of the results

We proceed in this section with a discussion of the effects observed in the simulations and providing an explanation of

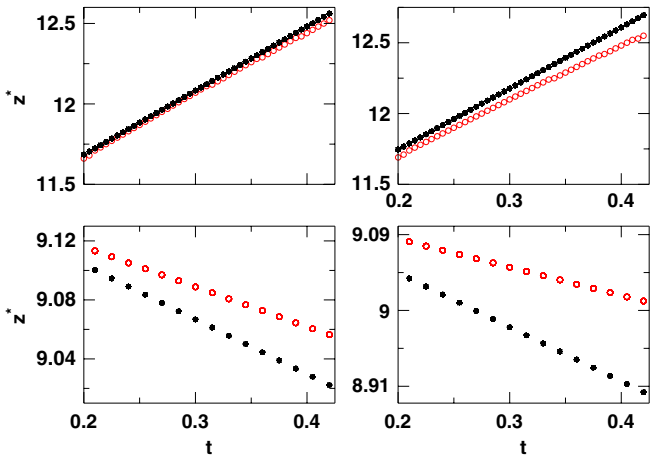

Figure 7. The same as in figure (5), with fixed σ and corresponding values of n_0 fulfilling equation (51) when $\Delta = 10^{-3}$ (left panels) and $\Delta = 6 \times 10^{-3}$ (right panels).

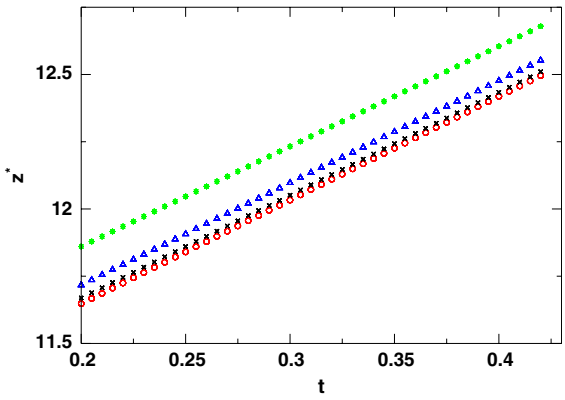

Figure 8. Evolution of $z^\star$ when photoionization is absent and the random term of the initial condition is restricted to a narrow interval around z_0. The different values of the intensity of the fluctuation term are: $\Delta = 10^{-5}$ (empty circles), $\Delta = 10^{-2}$ (crosses), $\Delta = 10^{-1}$ (triangles), and $\Delta = 1$ (full points). See text for details about the rest of the parameters.

the role played by fluctuations in the enhancement of the speed of the fronts.

In previous works [13, 17–19], it has been shown that the tail of the distribution of the charge ahead of the front plays a fundamental role in the dynamics of the front. The particular shape of this tail is not relevant, only its decay far away from the front. When the photoionization term is present, the characteristic ionization length of the photons extends the relaxation region of the tail, and the front moves faster. This is exactly the effect that fluctuations play when they are present. We will not perform here a rigorous mathematical proof of this statement, but we will instead show that this is the case with the following numerical experiment.

We consider again our streamer discharge model in the absence of the photoionization term and in the presence of an initial distribution of the form given in equation (41). The deterministic part will obey equation (42) but, in contrast to previous sections, the random term will be considered equal to equation (43) only in a certain interval $[z_0 - \delta z, z_0 + \delta z]$, being zero outside this region around the maximum of the initial charge distribution. In this way, we introduce an artificial cutoff in the random term which eliminates the contribution of charge fluctuations to the tail of the distribution charge. The results corresponding to the average position of the front as a function of time, $z^\star(t)$ are depicted in figure 8 for several values of Δ and $\delta z = 1$ (in all the simulations, z ranges from 0 to 20). Other parameter values remain as in figure 5. These results clearly show that the velocity of the front is the same in all cases, even for high values of Δ, although the value of the electron density for a fixed value of the space coordinate z increases as Δ increases, as expected.

So the charge fluctuations make the front speed up only when they are not restricted to a region close to the initial seed. It is claimed that the streamer develops out of an initial seed produced in a region where the field is high enough to produce an electron avalanche. We have shown that the charge produced in other regions may not be enough to initiate a streamer, but its presence definitely affects the dynamics of the streamer.

8. Conclusions

In this paper we have studied the effects of charge fluctuations on the propagation of streamer fronts. Whatever the origin of the fluctuations in a real discharge, they can play the same role as photoionization. We have shown that the fluctuations can make the front move faster.

We have modelled the fluctuations by introducing random initial conditions into a widely used minimal model for simulating the streamer propagation. We started from a general model and deduced the minimal one which retains the relevant physics for the range of parameters considered. The average behaviour of positive and negative fronts is investigated. The numerical experiments show that the random charge speeds up the front movement. Special attention has been paid to discard the effect of adding extra amount of charge when compared with the deterministic case.

The results are qualitatively analysed in the light of some theoretical predictions, and further numerical simulations are carried out to prove that the presence of charge fluctuations extended to the whole space along the streamer path accelerates the front. This effect definitely plays an important role in streamer dynamics. Moreover, its effect on the dynamics of the streamer is equivalent to the effect of photoionization.

We note that in pure gas discharges such as nitrogen or argon, the presence of photons able to ionize the gas is not so well understood as in oxygen–nitrogen mixtures. We want to remark that the presence of charge fluctuations in electric discharges is similar to the presence of impurities on semiconductors. The drastic effects of those impurities in the properties of semiconductors are well known. In this paper we have demonstrated that charge fluctuations indeed make the streamers move faster. This fact deserves further theoretical and experimental investigations.

Acknowledgments

MA and JLT acknowledge support from the Spanish Ministerio de Educación y Ciencia under project ESP2007-66542-C04-03.

JPB acknowledges support from the Universidad de Huelva (project FQM-276) and from the Universidad de Sevilla under the 'Ayudas de Extensión Universitaria' program, which made possible a research stay of Professors M Arrayás and J L Trueba at the Departamento de Física Aplicada II, where part of this work was done.

References

[1] Arrayás M and Trueba J L 2005 Investigations of pre-breakdown phenomena: streamer discharges *Contemp. Phys.* **46** 265–76

[2] Raether H 1939 Die Entwicklung der Elektronenlawine in den Funkenkanal *Z. Phys.* **112** 464–89

[3] Loeb L B 1936 The problem of the mechanism of static spark discharge *Rev. Mod. Phys.* **8** 267–93

[4] Liu N and Pasko V P 2004 Effects of photoionization on propagation and branching of positive and negative streamers in sprites *J. Geophys. Res.* **109** A04301

[5] Zhelezniak M B, Mnatsakanian A Kh and Sizykh S V 1982 Photoionization of nitrogen and oxygen mixtures by radiation from a gas discharge *High Temp.* **20** 357–62

[6] Kulikovsky A A 2000 The role of photoionization in positive streamer dynamics *J. Phys. D: Appl. Phys.* **33** 1514–24

[7] Pancheshnyi S, Nudnova M and Starikovskii A 2005 Development of a cathode-directed streamer discharge in air at different pressures: experiment and comparison with direct numerical simulation *Phys. Rev.* E **71** 016407

[8] Bourdon A, Pasko V P, Liu N, Célestin S, Ségur P and Marode E 2007 Efficient models for photoionization produced by non-thermal gas discharges in air based on radiative transfer and the Helmholtz equations *Plasma Sources Sci. Technol.* **16** 656–78

[9] Liu N, Célestin S, Bourdon A, Pasko V, Ségur P and Marode E 2007 Application of photoionization models based on radiative transfer and the Helmholtz equations to studies of streamers in weak electric fields *Appl. Phys. Lett.* **91** 211501

[10] Pancheshnyi S 2005 Role of electronegative gas admixtures in streamer start, propagation and branching phenomena *Plasma Sources Sci. Technol.* **14** 645–53

[11] Dhali S K and Pal A P 1988 Numerical simulation of streamers in SF_6 *J. Appl. Phys.* **63** 1355–62

[12] Vitello P A, Penetrante B M and Bardsley J N 1994 Simulation of negative-streamer dynamics in nitrogen *Phys. Rev.* E **49** 5574–98

[13] Arrayás M, Fontelos M A and Trueba J L 2006 Photoionization effects in ionization fronts *J. Phys. D: Appl. Phys.* **39** 5176–82

[14] Arrayás M 2004 On negative streamers: a deterministic approach *Am. J. Phys.* **72** 1283–9

[15] Naidis G V 2006 On photoionization produced by discharges on air *Plasma Sources Sci. Technol.* **15** 253–5

[16] Arrayás M, Fontelos M A and Trueba J L 2005 Mechanism of branching in negative ionization fronts *Phys. Rev. Lett.* **95** 165001

[17] Arrayás M, Fontelos M A and Trueba J L 2005 Ionization fronts in negative corona discharges *Phys. Rev.* E **71** 037401

[18] Ebert U, van Saarloos W and Caroli C 1997 Propagation and structure of planar streamer fronts *Phys. Rev.* E **55** 1530–49

[19] Arrayás M, Fontelos M A and Trueba J L 2006 Power laws and self-similar behaviour in negative ionization fronts *J. Phys. A: Math. Gen.* **39** 7561–78